Applicability of the Sensor Network Simulator Tool Suite for Proximity Operations

M. Schubert
Institute of Space Systems, Germany,
C. Kebschull, **N. Eggen**
OKAPI:Orbits GmbH, Germany
S. Silvestri
Institute of Space Systems, Germany

ABSTRACT

Ensuring the success of satellite missions and mitigating the risk of further in-orbit fragmentations require an awareness of the space domain that can keep pace with the growing number of objects that have to be observed by sensors, such as telescopes, radars, or laser ranging stations. In this context, tools to analyze and simulate sensor networks to observe objects in Earth's orbit can prove highly valuable. Recent activities at the Institute of Space Systems of the Technische Universität Braunschweig are oriented towards an expansion of the Sensor Network Simulator (SNS) tool suite to support such analyses. Within this work, the current state of the SNS is presented, detailing the individual tools in the toolkit and their respective capabilities and limitations. Additionally, a selection of previous results is included to provide further insights into the functionalities of the single sub-tools and the spectrum of results that can be obtained. Finally, as an appropriate exemplary utilization, preliminary analyses regarding the support of proximity operations in orbit are shown. For this purpose, the growth of state uncertainties over time between precise orbit determination data of real satellites and the propagator used within the SNS is studied. The goal of these analyses is to determine relevant sensor network parameters and requirements that are needed for the support of proximity operations and the connected need for high state accuracies.

1. INTRODUCTION

Considering a continuously growing object population in Earth's orbit, the importance of comprehensive Space Situational Awareness (SSA) is steadily increasing at the same time. Growing object numbers that have to be observed through ground- or space-based sensors, such as telescopes, radars, or laser ranging stations demand an appropriate awareness of the space domain. Only in this way the successful realization of satellite missions and mitigation of further in-orbit fragmentations can be ensured. To maintain an accurate and momentary awareness, these sensors have to keep pace with higher object numbers by increasing the capabilities to observe more objects with a sufficient frequency. Besides the necessity to build new sensor sites or increase the efficiency of existing sensor sites, more observations lead to a more extensive data flow that must be processed and compressed to accurate object catalogs. In this context, tools to analyze and simulate sensor networks to observe objects in Earth's orbit can prove highly valuable. They can be used to determine requirements and needs to build up and maintain object catalogs of high accuracy as well as to evaluate the performance of existing sensors and sensor networks.

Recent activities at the Institute of Space Systems of the Technical University Braunschweig have led to an expansion of the Sensor Network Simulator (SNS) tool suite to help with such analyses. Originally developed as the Radar

System Simulator, the SNS encompasses several core aspects needed to simulate the operations of an SSA system. Combining sophisticated performance models for optical and radar observations, the SNS allows simulations of complete sensor networks including radars and optical sensors that can be either ground- or space-based. In addition to propagating object populations and performing crossing, detection, and tracking analyses, the data can also be stored and post-processed subsequently. Hereby, the SNS allows the processing of the tracklets in various initial and precise orbit determination methods as well as post-processing of the catalog data in general, e.g. for the determination of the accuracy of the gathered object states.

Currently, the applications of the SNS in its updated state focus on simulating and evaluating existing sensor networks and investigating potential improvements in the efficiency of single sensors or sensor networks regarding SSA. In this context, sensor tasking algorithms are implemented and developed to optimize the use of the capabilities of different sensor sites.

In this work, an overview of the current state of the SNS will be presented. This will include detailed explanations of the single tools of the suite and their respective capabilities and limitations. It will further be laid out how these single tools work together to simulate the key aspects of object catalog build-up and maintenance. Further, a selection of previous results will be included to provide deeper insights into the functionalities of the single sub-tools and the spectrum of results that can be obtained. Finally, as an appropriate exemplary utilization, preliminary analyses regarding the support of proximity operations in orbit are shown. For this, the growth of state uncertainties between real data and propagated states is studied. The goal of these analyses is to determine relevant sensor network parameters and requirements that are needed for the support of proximity operations and the connected need for high object state accuracies. Such proximity operations are, for instance, needed when the mission of a spacecraft is the rendezvous with a space debris object for active debris removal. In-orbit servicing of satellites is another example of such proximity operations. Performing these activities requires knowledge about the momentary states of the spacecraft and target object with very high accuracy.

To provide the necessary context, Chapter 2 will start with a brief introduction into SSA and Space Domain Awareness (SDA) and the involved sensor types to observe objects in Earth's orbit and present the existing tools for Space Surveillance and Tracking (SST) simulations. Following this, the contents and capabilities of the SNS tool suite will be explained in Chapter 3. Additionally, exemplary results that have been obtained using the SNS or parts of it are included here. Preliminary analyses of the requirements on sensors or sensor networks for supporting proximity analyses and the corresponding results are shown in Chapter 4 and 5. Finally, a conclusion of the work is provided in Chapter 6.

2. BACKGROUND

SSA aims at gaining and keeping knowledge about human-made and natural objects close to the Earth or within an Earth orbit, including the environmental aspects influencing these objects. In addition to present-time awareness of the environment, projections into the future are essential to predict how that environment will develop. In general, SSA contains three aspects: SST, Space Weather, and Near-Earth Objects [1]. In addition to those aspects, SDA adds all aspects, such as human decision-makers and ground-based aspects, that influence the situation in space in any way [2]. This work focuses on object observations and orbit determination which are aspects of SST. To observe objects in space, ground- or space-based sensors are needed. These can be of different types, such as telescopes, radars, or laser ranging stations. How well the sensors perform regarding specific goals such as object catalog build-up and maintenance depends on many parameters. In order to test different sensor or sensor network designs and their performance, appropriate simulation tools are helpful. The existing tools for this purpose will be presented in the following section.

2.1 Existing SST tools

During the past years, multiple tools have been developed by different research institutions and companies that fulfill similar tasks as the SNS. An overview of the existing tools as of Spring 2023 can be found in [3] and only a brief summary will be provided here to give a comprehensive context for the presentation of the SNS and its capabilities. An additional tool developed by the S3TOC (Spanish Space Surveillance and Tracking Operations Center) for the evaluation of SST systems is not described in the following paragraphs as the authors were unable to find comprehensive documentation on it.

Ansys STK

Ansys, a company specializing in digital mission engineering, offers two products: Systems Tool Kit (STK) and Orbit Determination Tool Kit (ODTK). ODTK focuses on processing tracking data and orbit determination, while STK offers various options, including the analysis of electro-optical, infrared, and radar system performances [4, 5]. STK models different radar types, including space-based radars, and is used for radar system design, interference analysis, and optimal radar placement [5]. The main use cases for radar system design involve considering factors like Doppler shift, signal-to-noise ratio, detection probability, and optimal radar system placement. It also simulates up to 12 optical sensors, aiding in sensor system development and image analysis methods [4].

SSTAN

Deimos developed the SSTAN (SST Analysis Tool) for ESA, comprising various interconnected models to evaluate SST systems and their performance. SSTAN's modules encompass modeling the SST environment, sensor simulations, catalog building, and SST system analysis. The environment modeling module further divides into sub-modules for generating object populations, fragmentations, measurements, and post-processing the simulated data. The generated catalog allows for various analyses, including re-entries, collision risks, and maneuver identification. The measurement generation module of SSTAN allows simulation of radar and optical measurements, with various modes for radar and customizable strategies for optical measurements [6].

SPOOK

In 2019, Airbus Defence and Space presented SPOOK (Special Perturbations Orbit determination and Orbit analysis toolKit, previously SPace Object Observations and Kalman filtering), a tool designed to evaluate SST systems [7, 8]. The tool consists of three layers: simulation, analysis, and interface. It is capable of simulating both ground- and space-based optical and radar sensors, operating in various modes such as surveillance, tracking, or user-defined observation. SPOOK generates measurements, performs correlation, and can also simulate light curves and determine object attitudes and shapes [7, 8, 9]. Furthermore, the Airbus Robotic Telescope, deployed in Spain's Extremadura region in 2018, enables direct validation of SPOOK with real-world data [10].

SORTS++

SORTS++ (Space Object Radar Tracking Simulator) is an additional toolbox suitable for simulating various SST applications. Although initially developed in close collaboration with the EISCAT_3D radar system, it has the versatility to simulate different user-defined ground-based radar systems. The toolbox can effectively generate a space object catalog and incorporates ionospheric effects through ray tracing and the international reference ionosphere 2009 model [11].

BAS3E

BAS3E (Banc d'Analyse et de Simulation d'un Systeme de Surveillance de l'Espace – Simulation and Analysis Bench for a Space Surveillance System) is a CNES-owned tool with the primary goal of advancing existing SST networks [12]. It starts with a user-defined object population, such as the MASTER (Meteoroid and Space Debris Terrestrial Reference Model) or TLE (Two Line Elements) population, and can generate fragmentation objects using the NASA breakup model. The tool simulates observations using ground- or space-based radar and optical sensors, allowing for mono- or bistatic radar systems and surveillance or tracking modes for optical sensors. Measurement data is evaluated, and correlation and orbit determination methods are employed to determine object states. The generated data can then be used to build synthetic catalogs and further calculate collision risks. BAS3E has been validated with the French GRAVES (Grand Réseau Adapté à la VEille Spatiale) radar system [12].

SENSIT

The Italian SENSIT (Space Surveillance Sensor Network SImulation Tool) software, similar to previously mentioned tools, models sensor networks and evaluates their performance. It enables the creation and maintenance of space object catalogs and facilitates sensitivity analyses of sensor networks. Developed by Politecnico di Milano in collaboration with SpaceDyS and the Italian Space Agency, SENSIT comprises several key components, including data initialization, observable pass evaluation, catalog building, measurement simulation, orbit determination, performance analysis, and post-processing [13, 14, 15]. SENSIT is capable of simulating ground-based radars, whether mono- or bistatic, and optical sensors in both surveillance and tracking modes [15]. Additionally, it offers a scheduling tool that utilizes a genetic algorithm approach to resolve conflicts when a sensor might potentially observe two different objects simultaneously [13, 14].

3. STATE OF THE SNS AND EXEMPLARY RESULTS

The work on the SNS, formerly known as Radar System Simulator [16], was initiated in 2015 with the primary objective of studying and evaluating various SST setups, spanning from the sensor to catalog generation [17]. At the outset, the focus was on developing a simulation software comprising five distinct tools:

- MWG (MessWertGenerator): Measurement value generation
- SMART (Sophisticated Module for the Analysis of Radar Tracklets): Orbit determination algorithms
- PROCOR (PROcess COoRdinator): Process coordination
- CAT (Catalog Analysis Tool): Catalog statistics
- CAMP (Catalog Maintenance and Pass prediction tool): Conjunction analysis and pass prediction

The MWG is responsible for generating measurements. Hereby, a Radar Performance Model (RPM) is used to simulate different tracking radar types, such as the Tracking and Imaging Radar (TIRA) or surveillance radars like the German Experimental Space Surveillance and Tracking Radar (GESTRA). For optical observations, an Optical Performance Model (OPM) is used to simulate telescopes in tracking or surveillance mode. SMART takes these generated measurements and processes them to determine orbits, which are then stored in a database. CAT, on the other hand, is utilized to extract quality information about individual ephemeris and the entire catalog. Finally, CAMP derives pass predictions and conjunction information, which can be utilized to prioritize the measurement generation in the MWG, as illustrated in Figure 1.

3.1 Measurement generation

The RPM was supplied by the Fraunhofer FHR (Fraunhofer Institute for High-Frequency Physics and Radar Techniques) to simulate different kinds of radar systems. It allows the creation of detections with different operational modes of radars in the SST context [18]:

- Mechanical Tracking
- Electronic Tracking
- Surveillance
- Track-while-scan.

The last mode allows the usage of one or multiple tracking beams while being in surveillance mode. Within the RPM, the MWG uses the location of sensors as well as performance parameters, such as the transmitted energy, wavelength, transmit and receive gain, pulse repetition frequency, pulse duration, the 3 db opening angle of the beam, false alarm probability, assumed measurement noise, and pulse integration settings.

Regarding the RPM, the MWG simulates the ground- or space-based sensors and objects in Earth's orbit on a millisecond timescale, as needed for the pulses of the radar. To account for the movement of the space objects the numerical

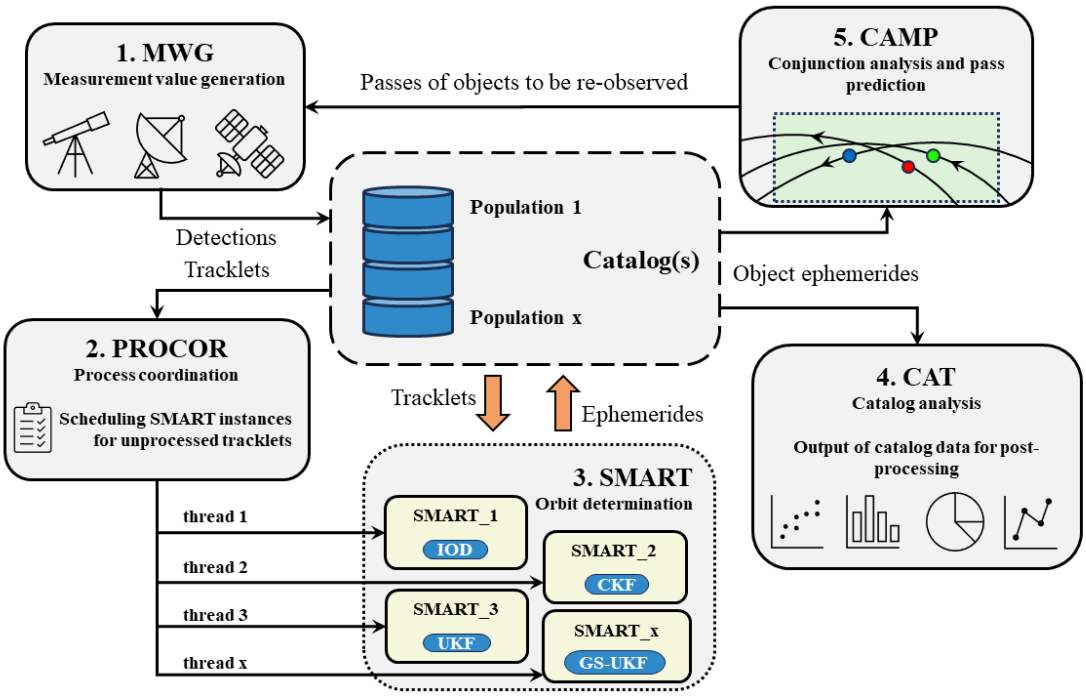

Fig. 1: Overview of the different tools contained in the SNS based on [16]

propagator NEPTUNE is used [19]. Ephemerides are generated, allowing the use of Chebyshev polynomials for interpolation of state vectors during the single radar pulses. The output of the RPM consists of noisy observation states, including range, range rate, azimuth and elevation, run time corrected time of the detection, and the signal-to-noise ratio (SNR). These observations are then stored in a database. When multiple observations of the same Resident Space Object (RSO) occur during a single pass over the sensor, they are grouped into tracklets.

The foundation for implementing the OPM was established by Krag in his work [20]. Following this dissertation, the simulation tool PROOF-2009 (Program for Radar and Optical Observation Forecasting) was developed which shares the same theoretical basis as the OPM of the SNS. While the primary purpose of PROOF-2009 is the support of validating the MASTER (Meteoroid and Space Debris Terrestrial Environment Reference) population and aiding in planning radar and optical observation surveys, the SNS serves as a tool to simulate complete sensor networks. Therefore, the OPM of the SNS was designed with a different focus and hence a different framework than PROOF-2009. Due to these distinct frameworks and purposes, significant differences exist in the implementations of the OPM within the SNS in comparison to PROOF-2009. The entire implementation of the OPM in the SNS consists of two key parts - the crossing analysis and the detection analysis, where the latter is the actual OPM. For the crossing analysis, the sensor and object positions are updated with an adaptive time step depending on the angular distance of the object from the FOV of the sensor. Once an object enters the FOV, the crossing uses a time step that ensures the generation of a user-defined number of crossing steps within the FOV. The object propagation and interpolation within the OPM are analog to the RPM. During the crossing analysis, all the crossings are saved and analyzed in the subsequent detection analysis.

For the detection analysis, it is generally assumed that the telescope uses a CCD as the detector and operates in the visible spectrum. Hereby, a complete CCD matrix is realistically modeled as a square matrix, whereby the user defines the pixel numbers, the linear pixel sizes, and the pixel scales, i.e. FOV per pixel. To determine if an object is detected by the CCD the SNR for each pixel is calculated taking into account the object's signal and the signal of multiple background sources. As background sources, bright stars and planets of the solar system are considered point sources, while faint stars, zodiacal light, airglow, galaxies, and atmospherically scattered light of the Sun, Moon, and other sources are considered continuous sources. The final detection decision itself relies on a straightforward threshold by which the object's signal has to exceed the background signal level [3, 20]. Besides the sensor location, the OPM uses several user-defined performance parameters, such as the diameter of the aperture, FOV, integration time, gap time,

threshold factor for detection, dark and readout noise, and the quantum efficiency of the sensor. For more details on the implementation please consider [3].

3.2 Orbit determination

Using the tracklets generated and stored in the database by the MWG, SMART conducts orbit determination to either establish an initial orbit or enhance the accuracy of the object's state. The tool retrieves the relevant observations for a specific object from the database and then processes them. Various methods for processing these observations, both for preliminary and statistical orbit determination, have been implemented, based on [21, 22, 23, 24, 25, 26, 27, 28, 29, 30]:

- Gibbs and Herrick-Gibbs
- Preliminary orbit determination method documented in the Goddard Trajectory Determination System (GTDS)
- Gauss iterative, Gooding, and Double-R angles-only methods
- Weighted Least Squares (WLS)
- Extended Kalman Filter (EKF)
- Unscented Kalman Filter (UKF)
- Cubature Kalman Filter (CKF)
- Ensemble Kalman Filter (EnKF)
- Gaussian Sum Kalman Filters (GS-UKF, GS-CKF).

Once a trajectory is successfully estimated, it is stored in the database. To accelerate the catalog maintenance process, multiple instances of SMART can run simultaneously which is especially beneficial when dealing with large object populations.

3.3 Process coordination

The PROCOR (Process Coordinator) tool utilizes multiple SMART instances to handle a continuous stream of incoming tracklets from one or more sensors. Filters can be applied, and settings can be passed to the SMART instances, ensuring the tracklets are processed optimally.

3.4 Catalog analysis

Using CAT, the accuracy of the cataloged states from individual objects can be compared with the true object state that is known to the MWG. Different states for the same object can be obtained and stored in the database by, e.g., using different precise orbit determination algorithms to improve the state accuracy. Thus preferable settings for specific situations can be found and used to improve the data that is contained in the catalog. Additionally, CAT can be used to derive statistics for bigger catalogs. The overall catalog quality or general accuracies for specific orbital regions or specific object types can be determined in this way.

3.5 Catalog maintenance

To fully simulate a sensor network and its use to build up and maintain an object catalog, CAMP fulfills two main purposes: pass prediction and conjunction screening. Both of these parts are important for the planning of re-observations. On the one hand, the pass prediction mode determines future passes of space objects through the FOV of a designated sensor. This information is valuable for scheduling the most favorable moments for conducting re-observations of specific objects. On the other hand, the conjunction screening mode aids in identifying critical objects that may be at risk of close approaches or collisions with other space objects. Such objects can then be given a higher priority for re-observations in order to increase their state accuracies and refine the conjunctions analyses. For the conjunction screening process, CAMP generates conjunction reports, which provide detailed information about the objects and their potential close encounters.

The numerical propagator NEPTUNE and a comprehensive library of essential functions used within the tool suite are openly accessible on GitHub [31, 32].

SNS in perspective

With multiple similar tools to evaluate sensor networks and to model key parts of SSA centers, it is useful to compare them and describe the strengths and weaknesses of the SNS within this context. In general, many of the features, such as modeling optical sensors and radars, building and maintaining catalogs, conducting orbit determination, and post-processing measurement data, are common among most of the tools. However, certain tools offer more specific functionalities beyond the common features. For example, SPOOK provides the ability to simulate light curves and determine object attitudes [8, 9]. Moreover, some tools offer the option to merge simulated and real data within a single catalog. Table 1 provides a comparison of the existing tools by listing specific capabilities and indicating whether each capability is present in a particular tool. The table is derived from available information about the individual tools, as well as a previous comparison from [3]. The term "user-defined population" refers to the user's ability to freely select the object population for simulations. "Network simulation" indicates the capability to configure entire networks, not just individual sensors. Additionally, "post-processing catalog data" refers to functionalities that, for example, provide users with object state accuracies for the objects listed in the catalog.

Table 1: Feature matrix for the previously presented tools. A checkmark means the feature is included within the tool and an *X* means it is not included. If the availability of a feature is not clear the entry is left blank. If the availability is provided partially then the checkmark is put in brackets [3, 4, 5, 6, 7, 8, 9, 10, 11, 12, 13, 14, 15].

Feature	**Ansys STK**	**SSTAN**	**SPOOK**	**SORTS++**	**BAS3E**	**SENSIT**	**SNS**
User-defined population		✓	✓		(✓)	✓	✓
Optical sensor simulation	✓	✓	✓	X	✓	✓	✓
Radar sensor simulation	✓	✓	✓	✓	✓	✓	✓
Infrared sensor simulation	✓	X	X	X	X	X	X
Surveillance & tracking	✓	✓	✓	✓	✓	✓	✓
Space-based sensors	✓	(✓)	✓	X	✓	X	✓
Network simulation	(✓)	✓	✓	✓	✓	✓	✓
Catalog build-up		✓	✓	✓	✓	✓	✓
Add real data to catalog			✓				✓
Orbit determination			✓		✓	✓	✓
Post-process catalog data		✓	✓		✓	✓	✓
Conjunction analysis	✓	✓	✓		✓		✓
Sensor scheduling			✓	(✓)	✓	✓	(✓)
Attitude identification		✓	✓				X
Weather effects, e.g, clouds	(✓)	X	X	X	X	X	X

The SNS's notable strength lies in its capacity to produce highly realistic and deterministic measurements using a range of sensor types that can be flexibly combined within user-defined sensor networks. As a result, the SNS proves valuable for simulating specific scenarios or sensor configurations and assessing their performance concerning measurement generation, catalog construction, and maintenance. Due to current efforts to include sensor scheduling algorithms within the framework of the SNS, the ability to evaluate specific sensor network configurations and potential increases in performance is further strengthened. At this point, the SNS lacks some of the more specific capabilities of other tools, such as light curve simulation, determination of object attitudes, and taking into account weather effects.

3.6 Exemplary results

During the past years, different aspects of SSA centers have been studied utilizing the SNS for a variety of simulations. To ensure the validity of the implemented RPM and OPM, simulations have been carried out using the algorithms that are implemented within the MWG. The results of these simulations have then been compared to real data. Further, orbit determination algorithms have been studied in detail. This includes sensitivity analyses of the performance of different orbit determination algorithms and analyses of different process noise methods. Additionally, an approach was made to define useful catalog metrics to determine the quality of the data within a specific catalog.

Validation of the RPM

The FHR Institute developed the RPM as stand-alone tool PROVE (Program for Radar Observation Vectors Estimation) and validated the results against real data from TIRA by [33]. Exemplary results for the LCS (Lincoln Calibration Sphere)-4 and Envisat are shown in Figure 2. The comparison shows that the RPM can reproduce the measurements for LCS-4 with a satisfactory level of accuracy. Also for Envisat the average SNR values are reproduced well, but the detailed development over time with many peaks and values can not be captured in detail. This is mainly due to the fact that the objects are modeled as spheres within the SNS and no attitude changes are considered.

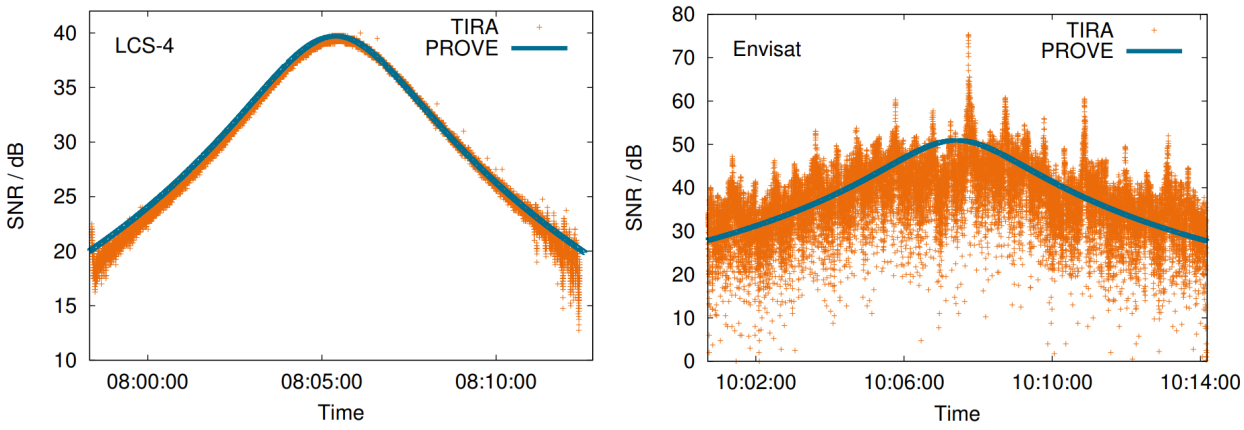

Fig. 2: Comparison between the SNR data obtained by TIRA and simulated using the RPM for LCS-4 (left) and Envisat (right) [33].

Validation of the OPM

The OPM was validated by using observations that were obtained in 2019 using an institute-owned Meade 10" LX200 telescope and a Canon EOS 6D camera. Hereby, observations of the satellites ALOS-2 and Meteor 1–29 were evaluated and subsequently reproduced using the SNS. As the basis for the simulations, TLE data has been used and the object states propagated until the time of observation [3]. Figures 3 and 4 show a comparison of the satellite pass using an SGP4 (Simplified General Perturbations) propagation as a reference, the observation by the telescope and the simulated values as generated by the SNS. It can be seen that the SNS simulations yield very similar results to the real data, while the visible differences can be explained by a camera timestamp (system time is considered for the taken images) that is only accurate to 1 s, the usage of TLE data as initial satellite states while the propagation was done using the NEPTUNE propagator, and a manually performed telescope calibration [3].

Since these figures only show the positional aspect of the observations, it was attempted to compare the simulated object magnitudes with the expected value of the real objects. Approximate values of objects during their passes for specific observer locations can be obtained from the website `https://heavens-above.com/` [34]. Table 2 shows a comparison of the expected magnitudes for ALOS-2 and Meteor 1-29 for the corresponding observation night and location as obtained from Heavens-Above (HA) and as obtained by the OPM of the SNS [3]. It can be seen that the simulated values for the object magnitudes are well within the expected range. For further details please refer to [3].

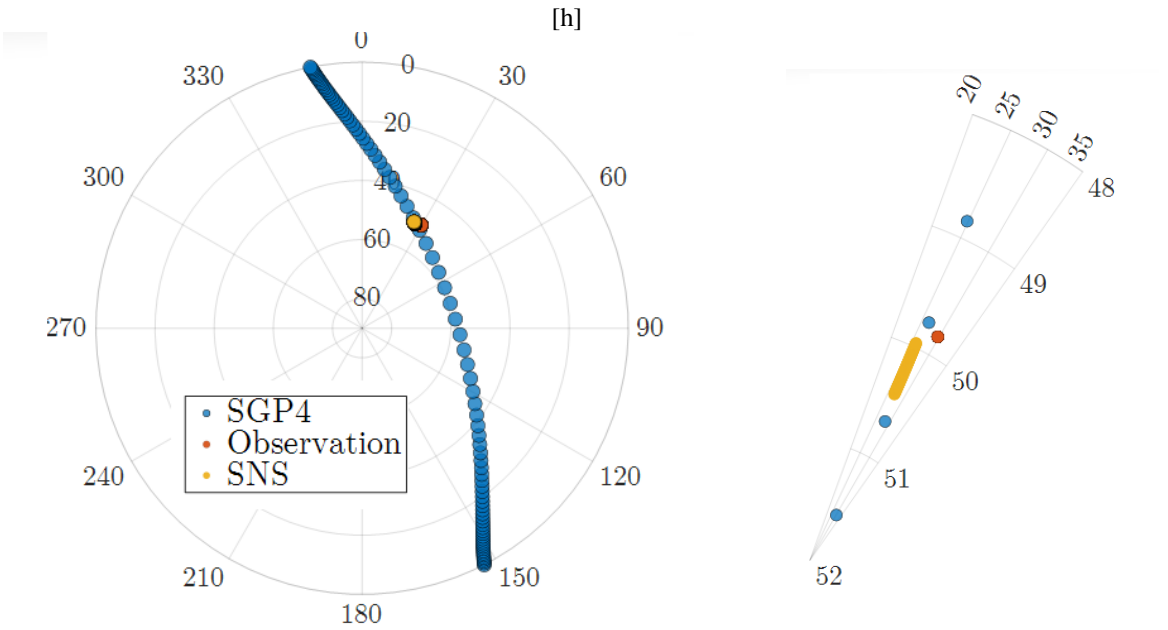

Fig. 3: Comparison between the observations obtained by the Meade 10” LX200 telescope and the simulations using the OPM of the SNS for the ALOS-2 satellite. The figure shows a complete skyplot (left) and a zoomed-version (right) [3].

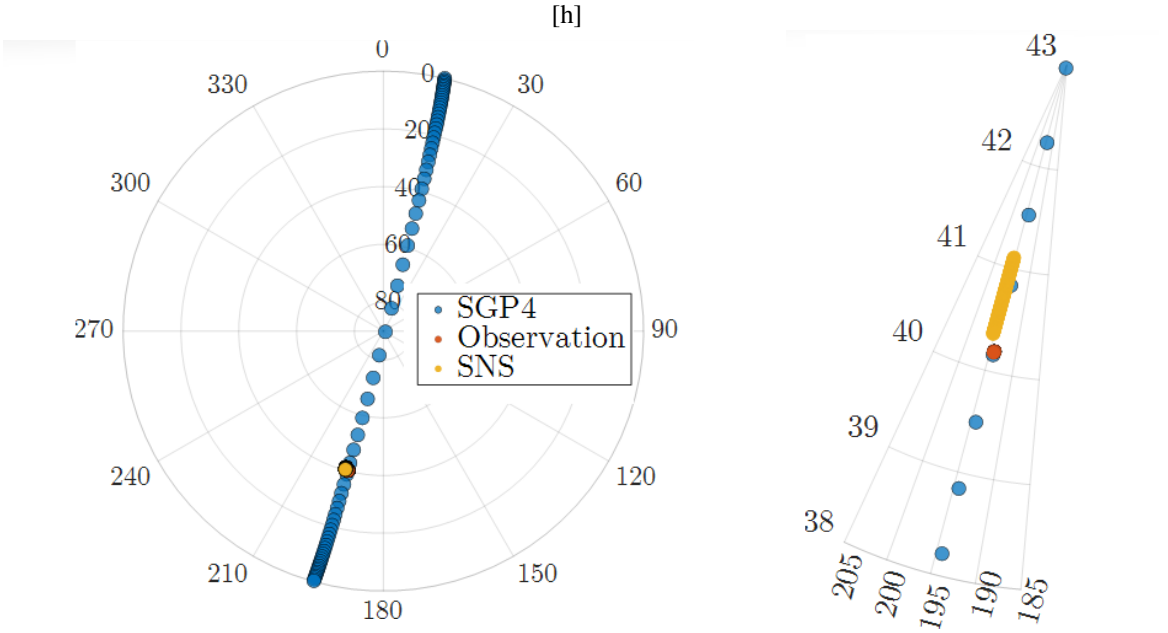

Fig. 4: Comparison between the observations obtained by the Meade 10” LX200 telescope and the simulations using the OPM of the SNS for the Meteor 1–29 satellite. The figure shows a complete skyplot (left) and a zoomed-version (right) [3].

Table 2: Comparison of the magnitudes of ALOS-2 and Meteor 1-29 as approximated by Heavens-Above (HA) and as simulated by the SNS. The passes took place on the 3rd of July 2019 [3].

	ALOS-2	Meteor 1-29
HA	2.7 – 5.0	3.7 – 5.3
SNS	4.1	4.6

Orbit determination and catalog quality metrics

The performance of orbit determination and the accuracy of the generated object states depend on the orbit determination method and multiple parameters, such as the data quality and quantity, the orbit of the object, or the physical properties of the object, e.g., the mass-to-area ratio. As described in Section 3.2 a variety of initial and precise orbit determination algorithms are available within the SNS. In sensitivity analyses, several of these algorithms were tested using the simulated observation data of different artificial object populations. For this purpose, object populations representing different orbital regions, different object sizes, and different mass-to-area ratios have been derived from the MASTER population. Table 3 shows the definition of the orbital regions that were used to generate populations containing objects in sun-synchronous orbits (SSO), polar orbits, low Earth orbits (LEO), geosynchronous transfer orbits (GTO), and Molnija orbits. Since the sensor parameters of TIRA were used for these simulations only objects passing LEO were chosen.

Table 3: Artifically selected populations for analyzing orbit determination methods for different orbital regions. Populations are derived from the MASTER population [35].

Orbit type	Number of objects	Diameter	Semi-major axis	Eccentricity	Inclination
-	-	m	km	-	deg
SSO	100	≥ 0.5	7125 - 7175	$\leq$0.01	97 - 101
Polar	100	≥ 1.0	6900 - 8000	≤ 0.1	82 - 92
LEO	100	≥ 1.0	6900 - 7400	≤ 0.1	0 - 90
GTO	100	≥ 1.0	23500 - 25500	≥ 0.5	0 - 50
Molnija	100	≥ 1.0	25000 - 28000	≥ 0.6	62 - 65

To generate observational data and tracklets as a basis for the orbit determination, the MWG was used to simulate observations of the different object populations with TIRA over a period of 24 hours. Using this data, a comparison of the results of the orbit determination using the Unscented Kalman Filter (UKF), the Extended Kalman Filter (EKF), and the Weighted Least Squares (WLS) methods is shown in Figures 5 - 7. These plots show the root-mean-square error (RSME) of the position of many objects, grouped in the described populations, as obtained by the UKF, the EKF, and the WLS respectively. It has to be noted that not all of the 100 objects of each population could be observed during the simulation period. This is especially true for the objects in a Molnija orbit leading to fewer data points in the shown plots. Additionally, a much higher number of tracklets and single detections have been obtained for the objects in polar, sun-synchronous, and low Earth orbits compared to the objects in Molnija orbits and GTO. This influences the orbit determination algorithms as they, generally, perform better with more data. From these exemplary results, different general observations can be made.

- The UKF achieves the highest accuracies for orbits with low eccentricities. For the majority of these objects, the RMSE is below 100 m
- The EKF performs comparatively badly with a wide range of relatively high errors for all orbital regions. For the majority of the objects, the RMSE is above 1 km. It performs best for polar orbits
- The results of the WLS have a lower variation overall. The majority of the objects have an RMSE between 80 m and 400 m. It achieves better results than the UKF and EKF for the orbital regions with high eccentricities, GTO and Molnija.

Such results can subsequently be used to optimize the usage of different orbit determination methods in order to achieve the best performance depending on the observational data.

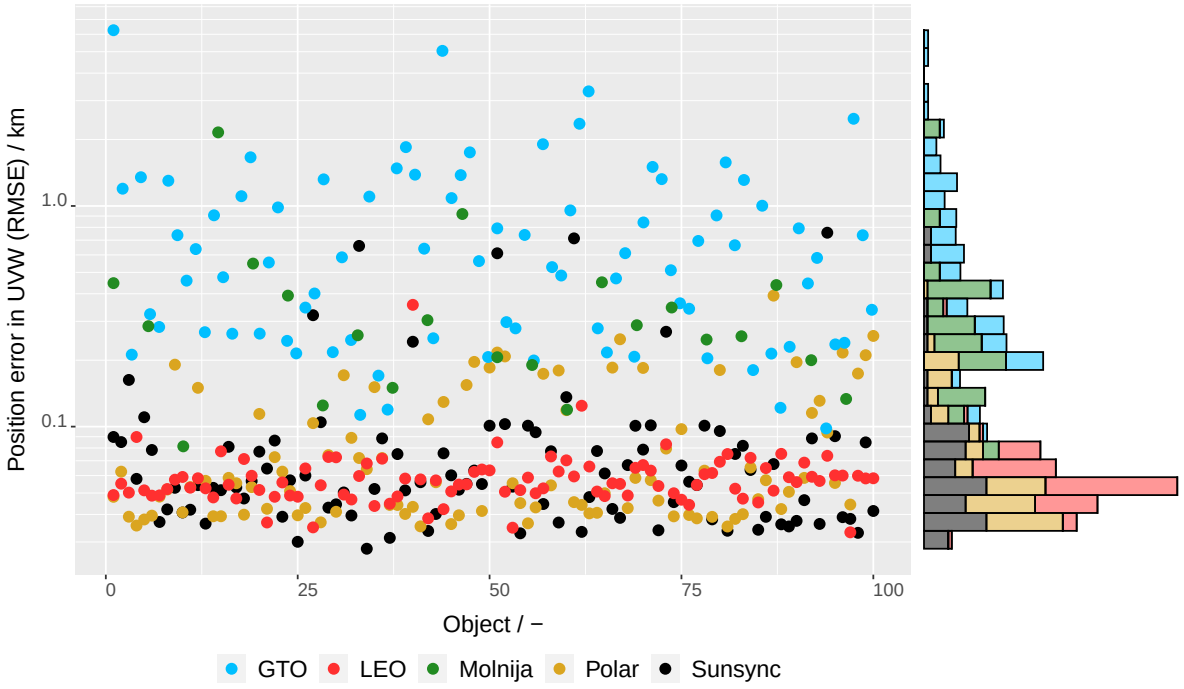

Fig. 5: Position error (RMSE) of the UKF in the object-centered UVW coordinates [36].

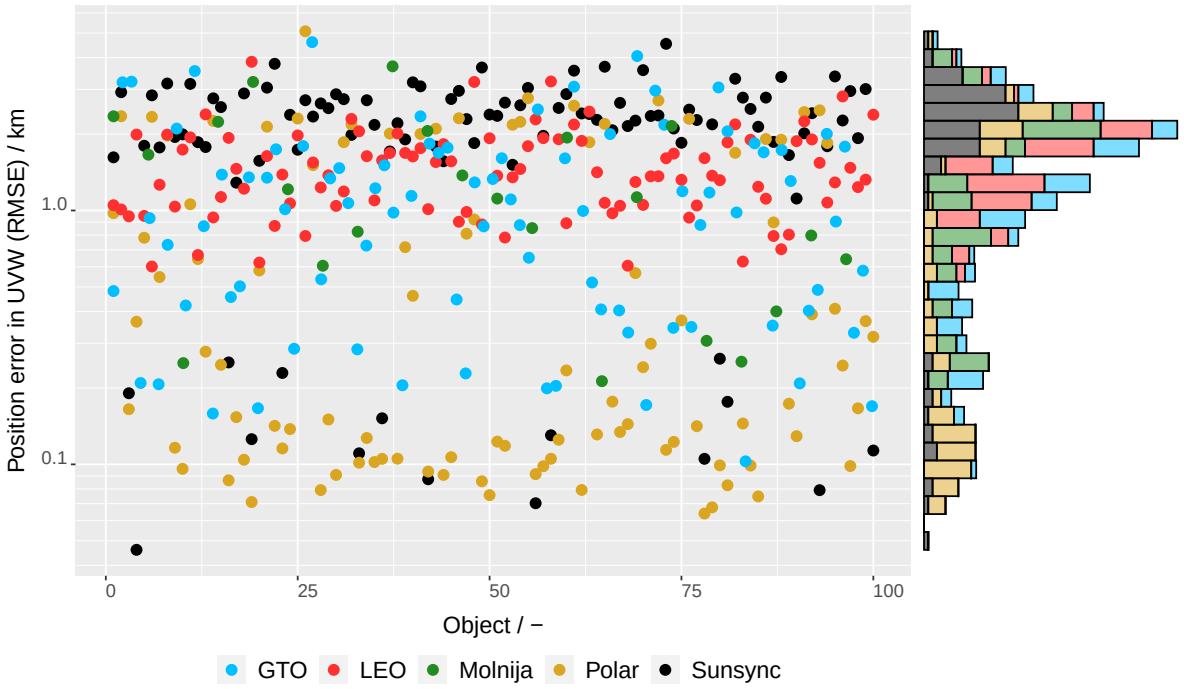

Fig. 6: Position error (RMSE) of the EKF in the object-centered UVW coordinates [36].

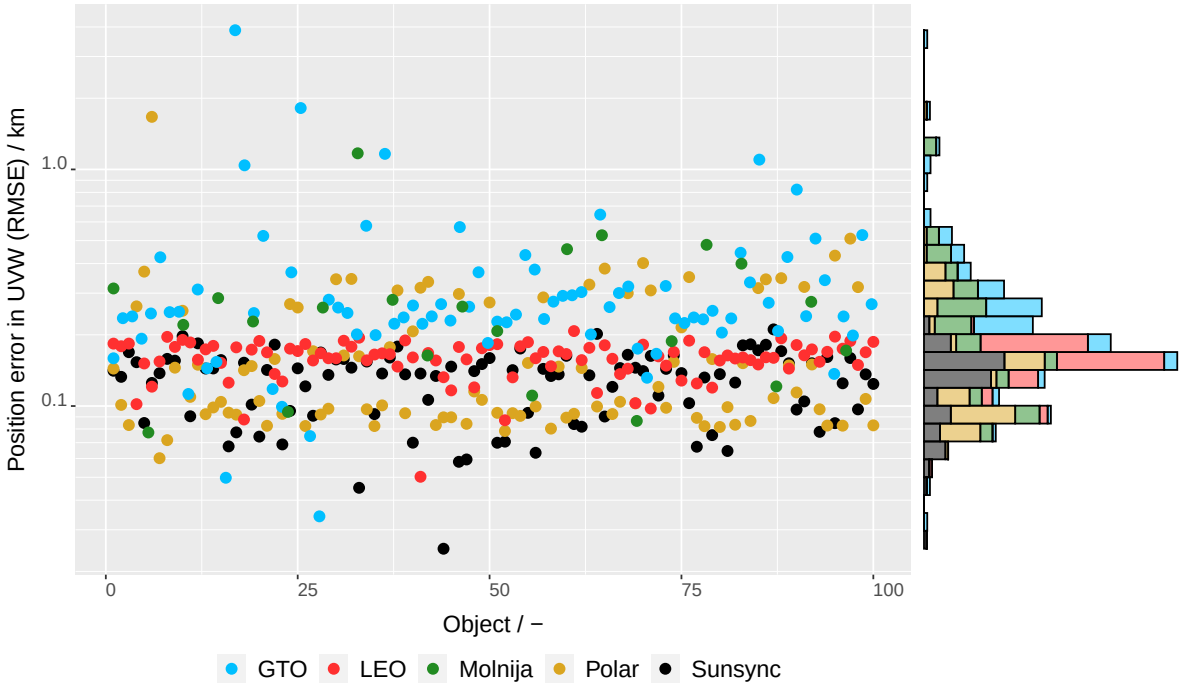

Fig. 7: Position error (RMSE) of the WLS in the object-centered UVW coordinates [36].

Further analyses of the performance of different orbit determination methods have been carried out using different process noise models to compensate for unknown errors, e.g., the models used for object propagation. Hereby, the process noise methods state noise compensation [37], covariance matching [38], and adaptive state noise compensation [38] have been evaluated in combination with different precise orbit determination methods. The main results of these analyses can be found in [35].

The MWG and SMART combine the simulation of measurement and tracklet generation with orbit determination in order to create or maintain object catalogs. Another important aspect is the evaluation of the data quality within the catalog. One approach is the utilization of reference values to create a relative metric for evaluating the state accuracies of the objects. To apply this method to the data generated with the SNS, expected standard deviations for objects within the TLE catalog of the US were determined by [39] for different orbits. The corresponding standard deviations can be used as reference values to derive a quality for the positional accuracy of single objects in the following way [36]:

$$q_u = \min\left(1, \beta \cdot \frac{\sigma_{u,ref}}{\sigma_u}\right) \quad q_v = \min\left(1, \beta \cdot \frac{\sigma_{v,ref}}{\sigma_v}\right) \quad q_w = \min\left(1, \beta \cdot \frac{\sigma_{w,ref}}{\sigma_w}\right), \tag{1}$$

where a value of 1 represents an equal or better quality with respect to the TLE catalog. The single components with subscripts u, v, and w represent the quality in the three coordinates of the object-centered UVW coordinate frame. The factor β can be used to allow further weighting with respect to the reference values. To obtain a single quality for the position of a cataloged object, the single components can be weighted equally and combined [36]:

$$q_{Pos} = \frac{1}{3} \cdot (q_u + q_v + q_w) \tag{2}$$

Calculating the quality for the accuracy of each object within the catalog allows the determination of a quality metric for the whole catalog by combining and weighing the single qualities as preferred.

4. PROXIMITY OPERATIONS

For the purpose of spacecraft docking, in-orbit inspection, and servicing, highly accurate positions of the involved objects must be known in the rendezvous phase (closing in from thousands of kilometers relative distance to hundreds

of meters). SST sensors (networks) support the operations of the servicer (or chaser) until reaching close proximity at which point spacecraft internal sensors (optical or radar) take over. There are several challenging aspects in these phases, especially for SST systems: (1) frequent maneuvers of the chaser may lead to bad OD solutions or even loss of the chaser (and target if it is moving as well) and (2) mis-correlation especially when both objects are getting close to one-another [40]. While there are requirements for SST providers, i.e. determining the frequent trackability of the target and chaser objects to take into account the changes of their trajectories over time, the operators in turn must share their maneuver plans to allow for proper tracking and subsequent OD solutions. One major impact apart from unknown maneuvers in the LEO is the atmospheric drag, which causes initial and within the propagation quickly developing uncertainties in the state vectors. Thus, to keep the uncertainties low, the servicer and the target need to be tracked frequently, such that the OD solution can be used as the basis for the maneuver close to the target. In the following the sensitivity toward different drag coefficients is shown, assuming mis-modeling of the solar activity that impacts the atmospheric model greatly, leading to errors in the assumed atmospheric density.

Data retrieval

The preliminary analyses performed in this work aim to show the growing deviations between the real satellite positions and the propagated positions over time. For this, publicly available POD data of the satellites Sentinel-1A and Sentinel-3A have been used. The corresponding data from April 2023 has been obtained from the Copernicus Sentinels POD Data Hub [41] for both of the satellites. The data has not been modified but transformed into the Geocentric Celestial Reference Frame (GCRF) and RTN (radial, in-track, normal) coordinate frame for easier comparison. For the exact starting point and the time span to be propagated, a period without maneuvers was selected from the maneuver histories for Sentinel-1A [42] and Sentinel-3A [43]. The same sources contain the spacecraft mass histories that were used to retrieve the corresponding masses for the selected time. A further parameter that is needed for the propagation is the cross-sectional area of the object in flight direction. These parameters could be retrieved from [44] and [45] for Sentinel-1A and Sentinel-3A respectively. The following Table 4 shows the data of the Sentinel satellites that are needed for the simulations.

Table 4: Initial parameters and states for Sentinel-1A and Sentinel-3A as used for the simulations [41, 42, 43, 44, 45].

	Start time in UTC	End time in UTC	Position in GCRF [km]	Velocity in GCRF $[\mathrm{km\,s^{-1}}]$	Mass [kg]	Cross-sectional area $[\mathrm{m^2}]$
Sentinel-1A	06.04.2023 22:59:42	12.04.2023 21:00:02	1291.421 -933.208 6883.720	1.733 -7.190 -1.297	2134.229	6.350
Sentinel-3A	05.04.2023 21:59:42	25.04.2023 21:59:42	-5951.171 1121.287 -3871.199	-3.627 2.038 6.173	1105.284	3.244

With an uncertainty of below 5 cm for the POD data of Sentinel-1A and below 3 cm for POD data of Sentinel-3A [46] the propagation can be started from an excellent initial point.

Simulation settings

For the comparison between the POD data of the two Sentinel satellites and the propagation results, the data from Table 4 was used as input for the NEPTUNE propagator. Further important input parameters concern the orbital perturbations that are considered. The following perturbation settings were used for the simulations:

- Geopotential up to the 85th term using the EIGEN-GL04C model
- Atmospheric drag using the NRLMSISE-00 atmosphere model
- Gravitational influences of the Sun
- Gravitational influences of the Moon

- Solar radiation pressure
- Earth albedo
- Solid Earth tides
- Ocean tides.

Additionally, the Earth orientation parameters as well as the effects on Earth's spin axis due to nutation and precession were considered. Finally, historical space weather data was used for the simulations.

5. RESULTS AND DISCUSSION

In the following, the results for the comparison between the POD data of Sentinel-1A and Sentinel-3A and the simulated position data are shown. Figures 8 and 9 show the temporal evolution of the position error in the RTN coordinate frame for Sentinel-1A over the whole simulation time of roughly 6 days and a zoomed-in version for the first day. Regarding Sentinel-3A, Figures 10 and 11 show, again, the temporal evolution of the position error in the RTN coordinate frame once over the full simulation period of roughly 20 days and a zoomed-in version for the first day. While the mass and cross-sectional areas of the satellites are known, the drag coefficient is one source of large uncertainty as it is unknown and significantly influences the orbital perturbations due to atmospheric drag. To analyze the sensitivity of the simulations with respect to the drag coefficient, several simulations were performed for both satellites with varying drag coefficients from 0.7 to 4.2, where a value of 2.2 was used as a reference value for Figures 8 - 11. The results of this analysis are shown in Figures 12 and 13 for Sentinel-1A and in Figures 14 and 15 for Sentinel-3A. The figures show the temporal evolution of the in-track error in the RTN coordinate frame once for the whole simulation time and once in a zoomed-in version for the first day.

In general, the radial and normal residuals oscillate with increasing amplitudes around zero while the in-track residuals grow continuously with time. During the first day of propagation, the in-track error grows to approximately 50 m for Sentinel-1A and approximately 100 m for Sentinel-3A. Continuing the propagation for many days without intermediate corrections leads to in-track errors of multiple kilometers.

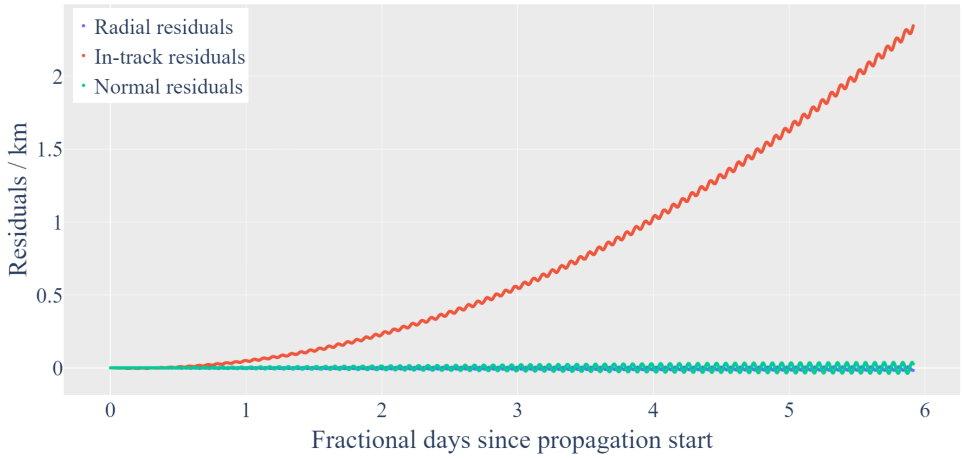

Fig. 8: Evolution of the position error between the POD data of Sentinel-1A [41] and the propagated position.

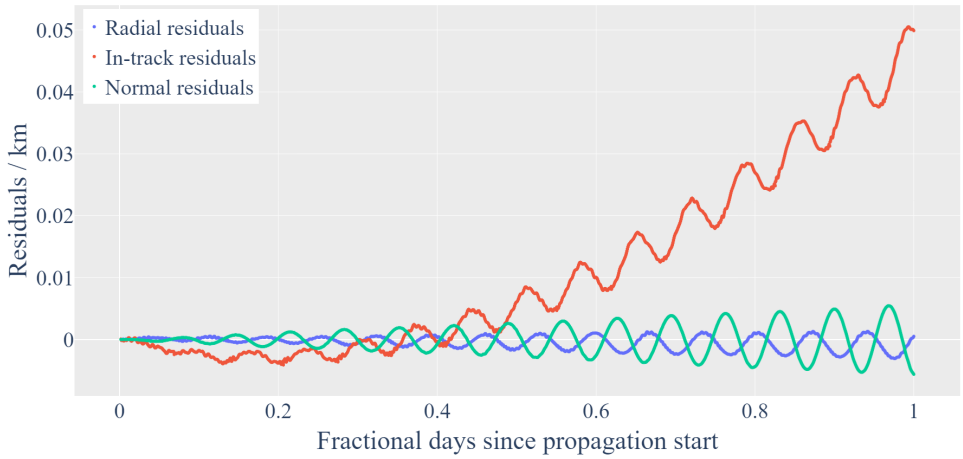

Fig. 9: Zoomed-in version of the evolution of the position error between the POD data of Sentinel-1A [41] and the propagated position over the first day.

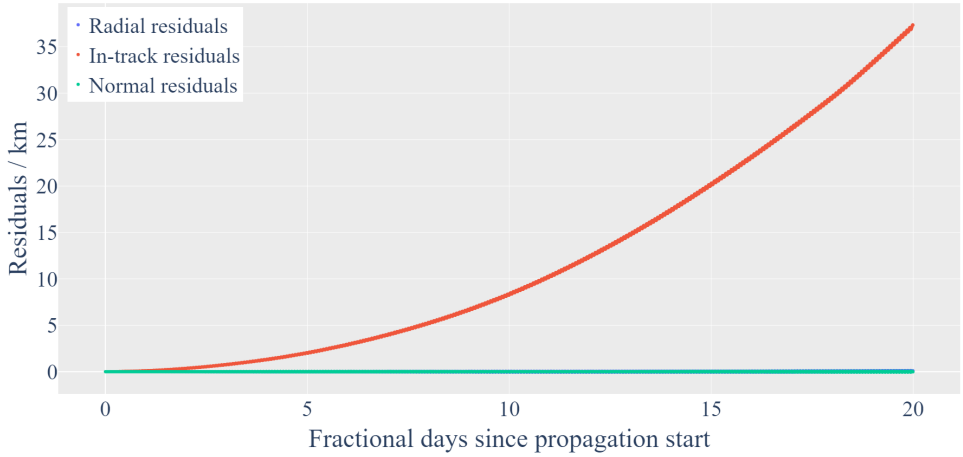

Fig. 10: Evolution of the position error between the POD data of Sentinel-3A [41] and the propagated position.

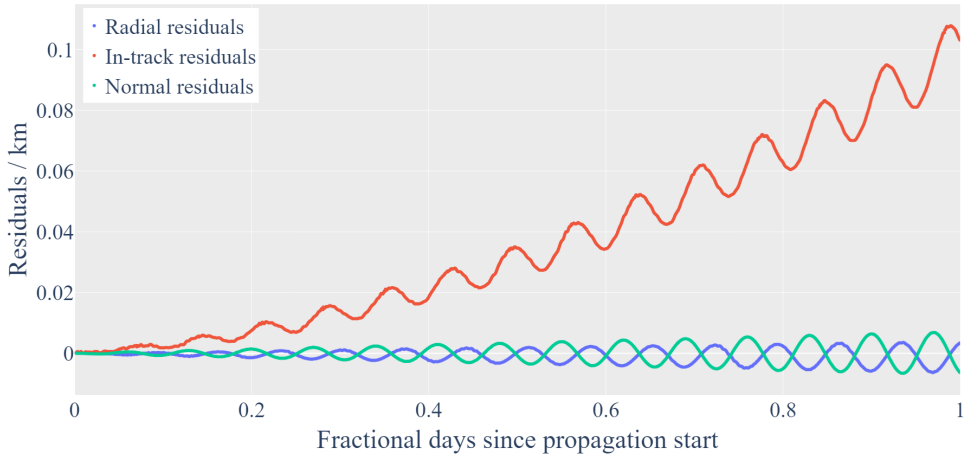

Fig. 11: Zoomed-in version of the evolution of the position error between the POD data of Sentinel-3A [41] and the propagated position over the first day.

Regarding the variations of the drag coefficient a large influence can be seen in the evolution of the residuals for Sentinel-1A and a much less but still significant influence can be seen for Sentinel-3A. As seen in Figure 13, the

in-track error for Sentinel-1A stays within ±8 m for the first day using a drag coefficient of 3.2, while the error growth rate increases proportionally to the difference from 3.2. For Sentinel-3A the growth rate of the in-track error is lowest for the highest simulated drag coefficient of 4.2 and highest for the lowest simulated drag coefficient of 0.7.

The scaling of the drag coefficient is analog to scaling the perturbational effects due to drag, while other influences, such as an imperfect atmosphere model and the exact cross-sectional area at each point in time, are not addressed. Since relatively high drag coefficients lead to the lowest in-track residuals, the perturbation due to drag might be underestimated in the reference case with a drag coefficient of 2.2. If this is due to the drag coefficient alone or a compensation effect cannot be concluded with certainty from the simulations. In principle, also other perturbational effects could be under- or overestimated and the increase of the drag coefficient could simply compensate for these inaccuracies, leading to better results.

For the given reference examples of Sentinel-1A and Sentinel-3A with a drag coefficient of 2.2, it appears to be possible to keep the in-track error below 50 to 100 m if updates with POD data are performed with an interval of at least 24 hours. For an interval of less than 12 hours, the error could be kept below 6 m for Sentinel-1A and below 35 m for Sentinel-3A. Slightly lower residuals can be achieved with varying drag coefficients.

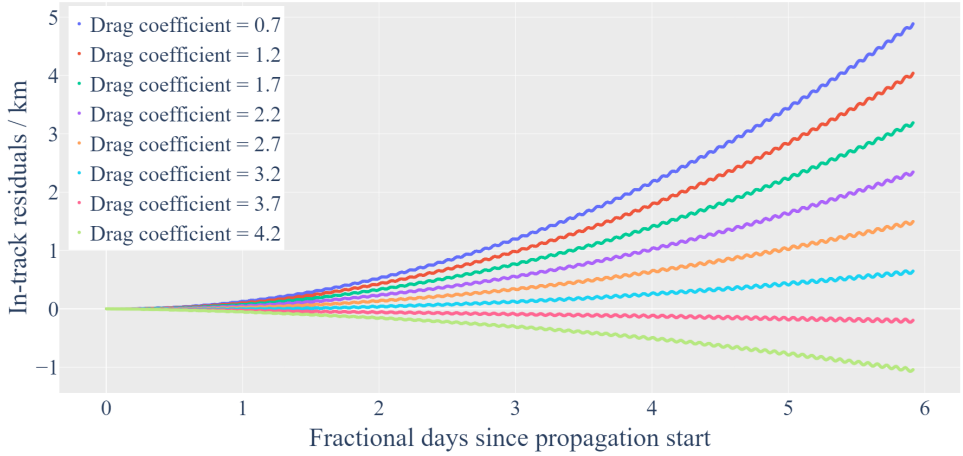

Fig. 12: Evolution of the position error between the POD data of Sentinel-1A [41] and the propagated position for different drag coefficients.

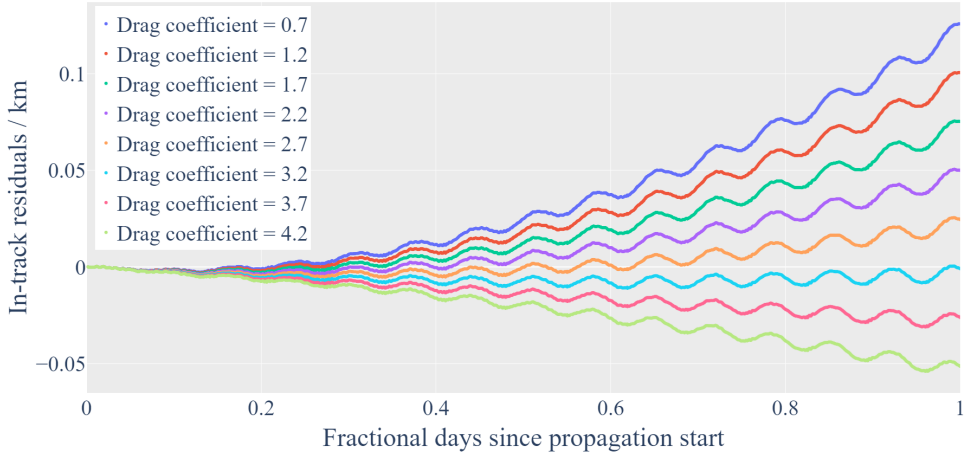

Fig. 13: Zoomed-in version of the evolution of the position error between the POD data of Sentinel-1A [41] and the propagated position for different drag coefficients over the first day.

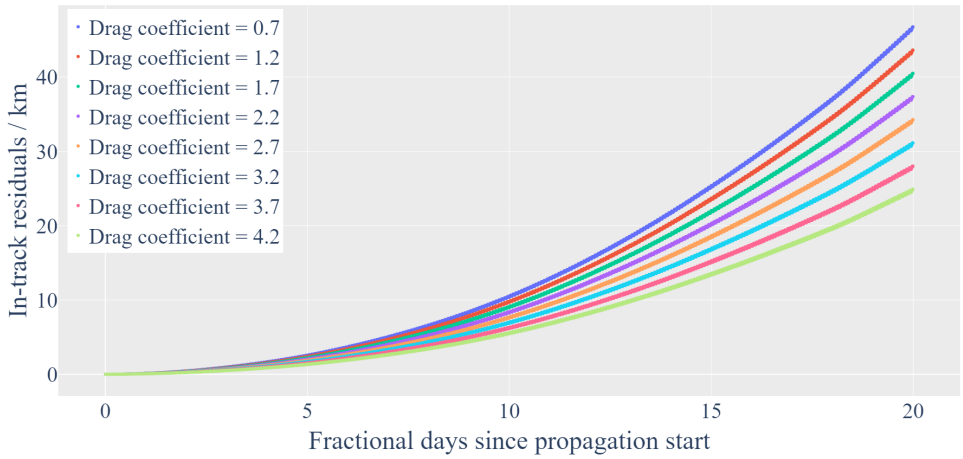

Fig. 14: Evolution of the position error between the POD data of Sentinel-3A [41] and the propagated position for different drag coefficients.

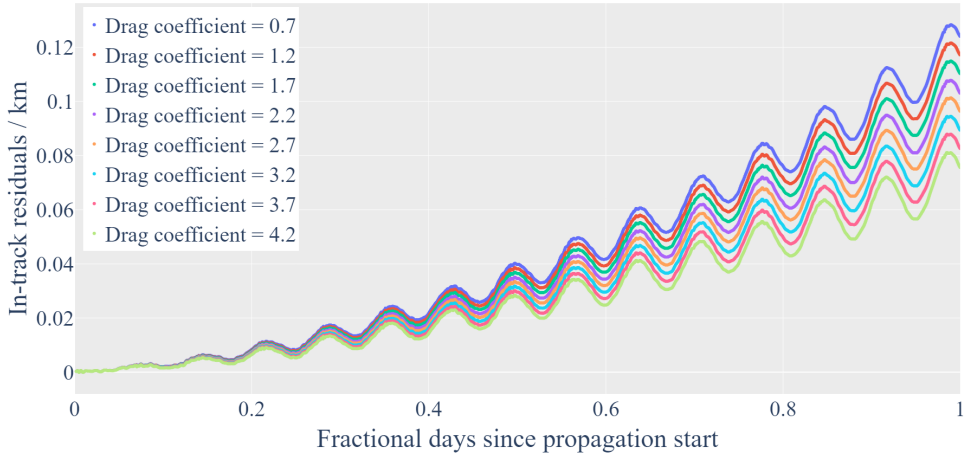

Fig. 15: Zoomed-in version of the evolution of the position error between the POD data of Sentinel-3A [41] and the propagated position for different drag coefficients over the first day.

While in-track errors of hundreds of meters can be too large for the direct support of proximity operations, the accuracies are low enough to guide the close approaches until the target is within range of the onboard sensors of the servicer. Following the close approach, onboard systems such as cameras can take over.

6. CONCLUSION

In this work, the SSN tool suite was presented in detail to provide an overview of its functionalities. To summarize, the simulation tool combines the different parts that are necessary for object catalog build-up and maintenance, such as object observation, orbit determination, and pass prediction for future observations. Further, the tools were compared to similar existing tools to point out the strengths and limitations of the SNS. For a deeper insight, exemplary results were included that show validation results for the RPM and OPM, exemplary analyses of different orbit determination algorithms, and an approach to define a metric for catalog data quality.

As an additional application of the SNS, preliminary analyses regarding the support of proximity operations using sensors or sensor networks were performed. For this, POD data of the two satellites Sentinel-1A and Sentinel-3A have been retrieved. They were, on the one hand, used as starting points to propagate the object's position using the NEPTUNE propagator. On the other hand, the POD data was then compared with the propagation results over approximately 6 days for Sentinel-1A and approximately 20 days for Sentinel-3A. Using a reference drag coefficient of

2.2 the in-track errors between the POD data and the propagation results increase to roughly 50 m in 1 day for Sentinel-1A and to roughly 100 m in 1 day for Sentinel-3A. The radial and normal residuals oscillate with slightly increasing amplitudes around zero. As a parametric analysis, the simulations were repeated using different drag coefficients between 0.7 and 4.2. Hereby, the in-track error evolution varies significantly with varying drag coefficients which indicates a considerable sensitivity of the propagation results concerning the perturbational effects due to drag forces. If the decisive parameter is the drag coefficient or other inaccuracies, such as the used atmosphere model, has to be further analyzed in future works. The results shown in this work and the evolution of the deviations between POD data and the propagated object positions can be used as indicators for the frequency with which observations of objects have to be performed to keep a certain position accuracy. In ongoing research, different sensor network scenarios are simulated using the SNS to confirm the preliminary results shown here. Further, the simulations are expanded to a larger number of satellites and additional parametric analyses.

7. ACKNOWLEDGEMENTS

The research leading to this manuscript was performed within three subsequent projects that were funded by the German Federal Ministry for Economic Affairs and Climate Action (Bundesministerium für Wirtschaft und Klimaschutz; before December 2021 it was named German Federal Ministry for Economic Affairs and Energy - Bundesministerium für Wirtschaft und Energie) under the funding codes 50LZ1404, 50LZ1803, and 50LZ2105. For the preliminary analyses regarding proximity operations, Copernicus Sentinel data from 2023 as provided by the Copernicus Sentinels POD Data Hub [41] was used.

[1] ESA. Ssa programme overview. `https://www.esa.int/Space_Safety/SSA_Programme_overview`, 2017. accessed at 26.07.2023.

[2] M. J. Holzinger and M. K. Jah. Challenges and potential in space domain awareness. *Journal of Guidance, Control, and Dynamics*, 41(1):15–18, 2018.

[3] M. Schubert and C. Kebschull. Enhancing the radar system simulator tool suite to allow the simulation of sensor networks. *Advances in Space Research*, 72(5):1538–1549, 2023.

[4] Ansys. STK Premium (Space) Advanced analytical tools and higher fidelity modeling in the space domain. *Ansys STK product brochure*, 2022.

[5] Ansys. STK Pro Modeling and simulation software for digital mission engineering and systems analysis. *Ansys STK product brochure*, 2022.

[6] R. Larisa Andrisan, N. Guijarro López, N. Sánchez-Ortiz, and T. Flohrer. SST analysis tool (SSTAN) supporting space surveillance and tracking (SST) services assessment. In *Advanced Maui Optical and Space Surveillance Technologies Conference (AMOS)*, April 2017.

[7] O. Rodriguez Fernandez, J. Utzmann, and U. Hugentobler. SPOOK - a comprehensive Space Surveillance and Tracking analysis tool. *Acta Astronautica*, 158(1):178–184, 2019.

[8] G. Pedone, D. Vallverdu Cabrera, M. G. V. Dimitrova, G. Cirillo, Y. Heinz, F. Schiemenz, and J. Utzmann. SPOOK: A tool for space objects catalogue creation and maintenance supporting space safety and sustainability. *Acta Astronautica*, 188(1):89–98, 2021.

[9] D. Vallverdu Cabrera, J. Utzmann, and R. Förstner. Inversion of the shape of space debris from non-resolved optical measurements within SPOOK. In *Advanced Maui Optical and Space Surveillance Technologies Conference (AMOS)*, September 2021.

[10] G. Cirillo, M. G. V. Dimitrova, J. Utzmann, Y. Heinz, G. Pedone, and D. Vallverdu Cabrera. Performance of airbus robotic telescope and the SST data processing framework SPOOK. In *8th European Conference on Space Debris*, April 2021.

[11] D. Kastinen, J. Vierinen, J. Kero, S. Hesselbach, T. Grydeland, and H. Krag. Next-generation space object radar tracking simulator: SORTS++. In *1st NEO and Debris Detection Conference*, January 2019.

[12] V. Morand, C. Yanez, J. C. Dolado Perez, C. Fernandez, S. Roussel, X. Pucel, and V. Vidal. BAS3E: A framework to Conceive, Design, and Validate Present and Future SST Architectures. In *First International Orbital Debris Conference*, 2019.

[13] G. Purpura, A. De Vittori, R. Cipollone, L. Facchini, P. Di Lizia, M. Massari, A. Di Cecco, and L. Salotti. GA-based optimal tasking for SST sensor networks in the SENSIT tool. In *73rd International Astronautical Congress (IAC)*, September 2022.

[14] G. Purpura, A. De Vittori, R. Cipollone, P. Di Lizia, M. Massari, C. Colombo, A. Bertolucci, A. Di Cecco, and L. Salotti. SENSIT: a software suite for observation scheduling and performance assessment of SST sensor networks. In *72nd International Astronautical Congress (IAC)*, October 2021.

[15] G. Purpura, A. De Vittori, R. Cipollone, M. Massari, C. Colombo, P. Di Lizia, S. Cicalo, F. Guerra, A. Bertolucci, A. Di Cecco, and L. Salotti. Development of a software suite for performance assessment of SST sensor networks. In *8th European Conference on Space Debris*, April 2021.

[16] C. Kebschull, A. Vananti, S. Flegel, S. Müller, S. Hesselbach, E. Gamper, J. Lorenz, and S. Horstmann. Schlussbericht, fkz: 50 lz 1404, radar system simulator. Technical report, Institute of Space Systems, 2019.

[17] C. Kebschull, L. Reichstein, and E. Stoll. A simulation environment to determine the performance of ssa systems. In *Advanced Maui Optical and Space Surveillance Technologies Conference (AMOS)*, September 2017.

[18] Sven K. Flegel. Program for Radar Observation Vector Estimation (PROVE) Software User Manual. Technical report, Fraunhofer FHR, 2015.

[19] Vitali Braun. *Providing orbit information with predetermined bounded accuracy*. PhD thesis, TU Braunschweig, December 2016.

[20] H. Krag. *A Method for the Validation of Space Debris Models and for the Analysis and Planning of Radar and Optical Surveys*. Shaker Verlag, 2003. Dissertation at the Technical University Braunschweig.

[21] P. R. Escobal. *Methods of Orbit Determination*. Krieger Publishing Company, 1997.

[22] A. C. Long, J. O. Capellari, C. E. Velez, and A. J. Fuchs. Goddard Trajectory Determination System (GTDS), Mathematical Theory, Revision 1. Technical report, NASA, July 1989.

[23] David A. Vallado and Wayne D. McClain. *Fundamentals of Astrodynamics and Applications*. Microcosm Press, fourth edition, 2013.

[24] R. H. Gooding. A New Procedure for Orbit Determination Based on Three Lines of Sight (Angles Only). Technical report, Defense Research Agency, 1993. Technical Report 93004.

[25] R. H. Gooding. A New Procedure for the Solution of the Classical Problem of Minimal Orbit Determination from Three Lines of Sight. *Celestial Mechanics and Dynamical Astronomy*, 66:387–423, 1996.

[26] W. F. Huseonica. A Numerical Evaluation of Preliminary Orbit Determination Methods. Technical report, National Aeronautics and Space Administration, 1970. NASA TN D-5649.

[27] I. Arasaratnam and S. Haykin. Cubature Kalman Filters. *IEEE Transactions on Automatic Control*, 54(6):1254–1269, 2009.

[28] K. K. Kottakki, S. Bhartiya, and M. Bhushan. State estimation of nonlinear dynamical systems using nonlinear update based Unscented Gaussian Kalman Filter. *Journal of Process Control*, 24:1425–1443, 2014.

[29] K. K. Kottakki, M. Bhushan, and S. Bhartiya. An improved Gaussian Sum Unscented Kalman Filter. In *Third International Conference on Advances in Control and Optimization of Dynamical Systems*, 2014.

[30] D. L Alspach. Gaussian Sum Approximations in Nonlinear Filtering and Control. *Information Sciences*, 7:271–290, 1974.

[31] Public GitHub repository of the NEPTUNE propagator. https://github.com/Space-Systems/neptune, 2023.

[32] Public GitHub repository of the libslam library. https://github.com/Space-Systems/libslam, 2023.

[33] S. Flegel, G. Bartsch, K. Letsch, L. Leushacke, T. Patzelt, C. Kebschull, and J. Gelhaus. Simulating noisy observation vectors for objects on earth orbits. In *Deutscher Luft- und Raumfahrt Kongress*, September 2015.

[34] C. Peat. Heavens above. https://www.heavens-above.com/, 2022. accessed at 25.10.2022.

[35] C. Kebschull M. Schubert and and S. Horstmann. Analysis of different process noise models in typical orbit determination scenarios. In *8th European Conference on Space Debris*, April 2021.

[36] M. Schubert, S. Horstmann, D. Cerutti-Maori, I. Maouloud, A. Vananti, J. Lorenz, and R. Lettmoden. Radar system simulator ii: Schlussbericht. Technical report, Institute of Space Systems, TU Braunschweig, 2022. Final report (funding code 50LZ1803).

[37] B. D. Tapley, B. E. Schutz, and G. H. Born. *Statistical Orbit Determination*. Elsevier Academic Press, 2004.

[38] N. Stacey and S. D'Amico. Adaptive and Dynamically Constrained Process Noise Estimation for Orbit Determination. *IEEE Transactions on aerospace and electronic systems*, 57(5):2920–2937, 2021.

[39] T. Flohrer, H. Krag, and H. Klinkrad. Categorization of TLE Orbit Errors for the US SSN Catalogue. In *Advanced Maui Optical and Space Surveillance Technologies Conference*, 2008.

[40] T. Harris, A. Lidtke, C. Pérez Hernández, A. Petit, F. Delmas, C. Jobic, D. Sáez Bo, and J. Fonseca. SSA observation campaign of the ELSA-D mission. In *73rd International Astronautical Congress (IAC)*, September 2022.

[41] Copernicus Sentinels POD Data Hub. https://scihub.copernicus.eu/gnss/#/home, 2023. accessed at 11.08.2023.

[42] European Space Agency. Satellite Parameters for POD. https://sentinels.copernicus.eu/web/sentinel/technical-guides/sentinel-1-sar/pod/satellite-parameters, 2023. accessed at 11.08.2023.

[43] European Space Agency. Satellite Parameters for POD. https://sentinels.copernicus.eu/web/sentinel/technical-guides/sentinel-3-altimetry/pod/satellite-parameters, 2023. accessed at 11.08.2023.

[44] M. Fernández. Sentinel-1 Properties for GPS POD. https://sentinels.copernicus.eu/documents/247904/3455957/Sentinel-1-properties-for-GPS-POD, 2019. accessed at 11.08.2023.

[45] M. Fernández. Sentinel-3 Properties for GPS POD. https://sentinels.copernicus.eu/documents/247904/3372613/Sentinel-3-GPS-POD-Properties.pdf, 2019. accessed at 11.08.2023.

[46] J. Fernández Sánchez. Copernicus POD Service File Format Specification. https://sentinels.copernicus.eu/documents/247904/351187/Copernicus_Sentinels_POD_Service_File_Format_Specification, 2022. accessed at 11.08.2023.